

Pit clustering in cavitation erosion

Matevž Dular*, Aljaž Osterman

Laboratory for Water and Turbine Machines, University of Ljubljana, Aškerčeva 6, 1000 Ljubljana, Slovenia

Received 12 March 2007; received in revised form 28 December 2007; accepted 8 January 2008

Available online 4 March 2008

Abstract

An investigation of the erosion effects of cavitation on a thin aluminium foil was made. Cavitation was generated in a small tank with capacity of about 500 ml of clean water. The growth and collapse of bubbles was triggered by means of ultrasound. The sustained damage was measured by evaluating the area of the damaged surface in time intervals of 4 s. Also the length of the boundary between the damaged and the undamaged surface and the characteristic pit/hole size were measured. The goal of the study was to investigate the phenomenon of pit clustering within the incubation period and the influence of the already eroded surface on appearance of new pits. Additionally, the possibility of self-amplification of the erosion due to the presence of small deformations (pits) was studied.

The results evidently show that pits tend to appear in clusters and near already damaged surface and this can be explained by the fact that the already present deformations on otherwise polished alloy surface act as the “cavitation generators” and cause more bubbles to appear and collapse in that region.

Determining the physics of these phenomena is of great importance for engineering applications (preventing erosion in water turbines, pumps, diesel engine nozzles, etc.), also because most studies, that deal with predicting the actual mass loss, investigate the erosion in the incubation period and then extrapolate the results to the time scale of a real machine operation (B. Bachert, G. Ludwig, B. Stoffel, S. Baumgarten, Comparison of different methods for the evaluation of cavitation damaged surfaces, ASME Fluid Engineering Division Summer Meeting and Exhibition, Houston, 2005; J.P. Franc, J.M. Michel, Fundamentals of Cavitation, Kluwer Academic Publishers, 2004).

© 2008 Elsevier B.V. All rights reserved.

Keywords: Cavitation; Erosion; Pit; Cluster; Self-amplification; Ultrasound

1. Introduction

Cavitation denotes appearance and collapse of bubbles in an initially pure liquid region due to the pressure fluctuations. It is considered as one of the most ubiquitous problems in hydraulic machines since it causes changes in flow kinematics, drop in machine efficiency, noise, thermal effects and probably the most important—the erosion of solid surfaces. There are various ways to generate cavitation—one of the simplest is to use ultrasonic excitation.

Ultrasonic devices that are used for generation of cavitation are mainly piezoelectric transducers. Excitation frequencies associated with cavitation effects usually lie in the range between 20 and 60 kHz [3,4]. Due to the inertia, the liquid cannot follow

the oscillations of the sound field, hence low-pressure regions in antinodes in vicinity of solid surfaces and elsewhere in the liquid repeatedly occur. If the pressure oscillations are high enough (if the pressure drops below the critical pressure), cavitation bubbles appear and collapse.

The phenomenon of cavitation erosion is complicated and its physical background is still not entirely clarified. There is still debate what is the sequence of events that leads to the formation of a pit (small plastic deformation) and consequently to material loss.

Basically there are two possibilities, but probably it is a combination of both that completely explains the phenomenon.

The first is the so-called micro-jet. A bubble positioned in the vicinity of the solid surface collapses asymmetrically. As this occurs, the fluid that surrounds the bubble takes a shape of jet through the bubble, directed towards the solid surface. Benjamin and Ellis [5] provided experimental proof of the micro-jet formation. Later on the process was theoretically approached by Plesset and Chapmann [6]. It was found that the liquid jet that

* Corresponding author. Tel.: +386 1 4771 453; fax: +386 1 2518 567.

E-mail addresses: matevz.dular@fs.uni-lj.si, matevz.dular@email.si (M. Dular), aljaz.osterman@fs.uni-lj.si (A. Osterman).

Nomenclature

A	damaged area (mm^2)
c	sonic velocity (m/s)
E	pixel grey level
f	ultrasound frequency (Hz)
i	pixel coordinate in the first direction
I	number of pixels in the first direction
j	pixel coordinate in the second direction
J	number of pixels in the second direction
k	scale of the image (mm/pixel)
L	length of the boundary between the damaged and the undamaged surface (mm)
n	antinode number
R	characteristic pit/hole size (mm)
x_{an}	antinode position (m)
<i>Greek symbol</i>	
λ	wave length (m)

penetrates the bubble can reach a velocity of several hundred m/s and can cause a shock with high local tension of the material [7].

The other explanation is that the damage, caused by the micro-jet, is marginal compared to the damage, caused by the spherical collapse of microbubbles that are either already near the surface or are generated during the so-called splashing effect [8]. After the micro-jet hits the surface, it spreads in thin film inside the boundary layer; consequently, microbubbles are generated due to friction between the liquid at rest and the moving remains of the micro-jet. In the case of microbubbles, the surface tension prevails, hence the collapse is spherical what leads to a powerful shock wave that damages the nearby surface.

We can distinguish two periods in the cavitation erosion process. The incubation period where only small plastic deformations (pits) can be seen. The pits are accumulating, but still no material loss is present. When enough pits accumulate conditions for material separation are ripe. So during the second period the material separates from the surface, first at an exponential and later at a linear rate [2].

For evaluation of cavitation erosion visual methods are most commonly used. Here a soft metal specimen (aluminium or copper) or a specimen coated with paint is exposed to cavitation [9–11]. The erosion is then evaluated according to the number, and the size of the pits [9]. The problem of this method is that it can be used only within the incubation period and even then too many pits can deform the results due to overlapping.

When the specimen endures many pits and is subjected to significant material loss, the erosion can only be evaluated by weighing the specimen or by interferometry [1]. These methods are less popular in research due to the very long time of needed observation (it took Bachert et al. [1] over 200 h of test rig operation to determine the representative erosion rate evolution for the case of a copper specimen—other materials are of course even more resistant to erosion). Also such studies are usually used

only for evaluation of the materials resistance to the cavitation erosion and not for studding the physics behind it [2].

On the other hand, one can visually evaluate the erosion throughout the process, when a thin metal foil is used as a sensor, since the material loss can be observed as small pieces of foil separate. The idea of using a metal foil for determining the erosion magnitude of ultrasound induced cavitation is not new and has been used by many authors [3,12,13], but it has not been used for a study of time evolution of erosion until now.

In the present study, cavitation was generated by means of ultrasound in a small cylindrical vessel. A thin aluminium foil was used as a sensor for cavitation erosion. During the operation of the ultrasonic bath, images of the foil were taken every 4 s. Evaluation of the images revealed that the pits first tend to form clusters. After the end of the incubation period, when parts of the foil are torn away and holes appear, the erosion concentrated to the already damaged region (to the edge of the holes), rather than form new pit clusters. The damage rate increased during that period which means that the presence of damage accelerates further erosion.

The results of the present study will help to determine the laws of extrapolation from a short time scale (laboratory measurement within the incubation period) to the real time scale (machine operation).

Contributions of this study can also be easily implemented in the models for CFD (Computational Fluid Dynamics) prediction of cavitation erosion where only a small time frame of the machine operation can be simulated.

2. Experimental set-up

Fig. 1 shows the experimental set-up.

A small cylindrical vessel, made out of stainless steel, with inner dimensions 120 mm high and 72 mm in diameter was used. Below it, a 50 W (intensity at the emitting surface was 2.54 W/cm^2) piezo actuator, that produced periodic oscillations at an ultrasound frequency, was mounted. The piezo actuator was connected to the power control unit.

A CCD camera was used to capture the images of the foil surface. The frequency of image capturing was 1 image per 4 s. The region of interest was resolved by about 1000×1000 pixels

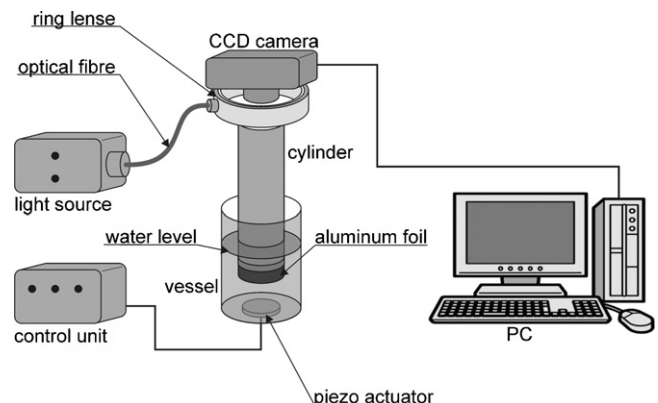


Fig. 1. Experimental set-up.

leading to resolution of 40 $\mu\text{m}/\text{pixel}$. The exposure time was 1/160 of a second, focal length was 18.3 mm and the focal ratio was set to 4.5. Images were saved in 8-bit greyscale mode that gives 256 levels of grey level ((0) black and (255) white).

The illumination was provided by a continuous light source VEGA VELUM150DR (lamp: EKE 21 V 150 W). The light was transmitted via optical fibre and was dispersed through a ring lens what enabled a brightly and evenly illuminated region of interest with very little unwanted reflection.

A 10 μm thick aluminium foil was used as erosion “detector”. It was mounted on a cylinder with inner diameter of 40 mm and submerged in a vessel. The water level inside the cylinder was the same as the level in the vessel. This prevented the possible flow from one container to another as holes were eroded in the foil, which could influence the results and also complicate acquisition of the images. The foil was positioned in the centre of the vessel at various distances from the bottom, that enabled us to adjust the aggressiveness of cavitation, as will be explained later. The level of water was always 20 mm above the position of the foil (foil was submerged to the depth of 20 mm).

Unprepared water was used for the experiments—the content of dissolved and undissolved gasses was measured with the van Slyke method [14] and was held almost constant at 27 mg of gas per liter of water. The uncertainty of the gas content measurements was $\pm 1\%$ of the measured value.

Since the vessel was open to the surroundings, the experiments were performed under constant atmospheric pressure of 985 mbar.

The water temperature remained approximately constant—it rose from about 22 °C at the beginning to approximately 24 °C at the end of each 800 s long experiment.

The ultrasound frequency of 41.5 kHz that caused water tank oscillations was measured with capacitive hydrophone Bruel and Kjaer type 8103, submerged in the water in the centre of the vessel.

3. Damage evaluation

Fig. 2 shows three typical situations during the experiment. Images a, b and c were taken 240 s apart (0, 240 and 480 s). The first image (a) shows the foil just after the start, where no damage can be seen. The second image (b) shows slightly damaged foil—in this case one can only observe plastic deformations (pits, dimples), but no actual penetration of the foil. The third image (c) shows eroded foil where the foil is penetrated and a significant part of the foil is torn away.

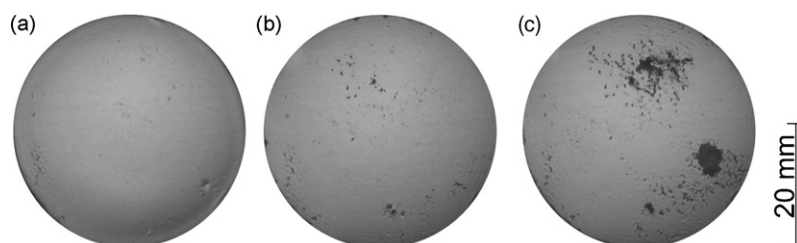


Fig. 2. Images of the foil: (a) undamaged foil, (b) plastically deformed foil, and (c) eroded foil.

The first image (a) does not need further description, while the other two do. The reason for the appearance of dark regions in the image is different for images (b) and (c). For the case of image (b), the dark regions appear as a result of small plastic deformations (pits) that cause the light to deflect from the direction of the camera. In the case of the eroded surface (c), the dark regions are in fact holes in the foil (we are looking into the darker space beneath the foil). It is essential, for further evaluation, to distinguish pits from holes (plastic deformations of the foil from the foil erosion) since the transition from one to another denotes the end of the incubation period (the moment when enough pits accumulate that a piece of the foil separates from the rest of it). It can, of course, occur that one region of the foil is still in the incubation period while the other already experiences “real” erosion.

In Fig. 3a we can see a magnified section of the foil where a hole and pits can be seen. For a clearer presentation a schematic cross-section through a hole and a pit is shown in Fig. 3b. There are two differences in appearance of a pit and a hole in the foil in an image.

1. a pit is smaller than a hole and has a relatively constant diameter between 0.15 and 0.25 mm,
2. the bottom of the pit lies approximately perpendicular to the light source, hence the light is reflected directly back to the camera, resulting in a very small bright region in the middle of a dark region (Fig. 3a and b).

3.1. Edge detection

The Sobel operator [15] was used to determine the boundary between the damaged and the undamaged surface. It performs a 2D spatial gradient measurement on an image. Typically it is used to find the approximate absolute gradient magnitude at each point in an input greyscale image. A typical result of such analysis can be seen in Fig. 4 where (a) shows the original image and (b) gives the detected edges.

If the scale at which the original image was taken is known (in this case $k = 40 \mu\text{m}/\text{pixel}$), the overall length of the boundary between the damaged and the undamaged surface can now be simply calculated by counting the black pixels in Fig. 4b:

$$L = k \cdot \sum_i^I \sum_j^J E(i, j) \quad \text{for } E(i, j) = 1, \quad (1)$$

where E is the value of the pixel (only pixels with value equal to unity $E(i, j) = 1$ (black pixels) are considered).

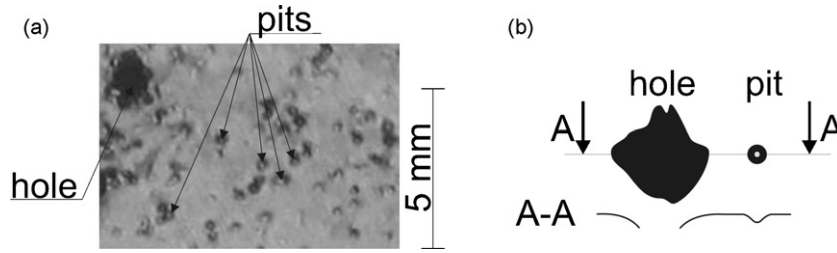


Fig. 3. Close-up of the foil surface—a hole surrounded by pits can be seen.

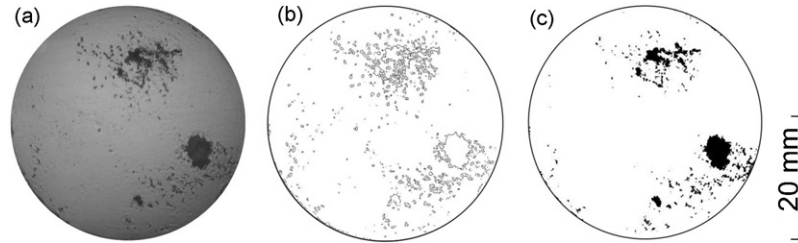


Fig. 4. Boundaries between the damaged and undamaged surfaces and the damaged area ((a) original image, (b) edges detected by Sobel algorithm, and (c) damaged area).

3.2. Determination of the size of the damaged area

As already mentioned, the dark regions in the image correspond to the damaged area (both pits and holes). Area of the dark region was used as the evaluation parameter. A threshold value of grey level was used to generate binary image where the damaged area can be clearly seen and evaluated. Fig. 4c shows the processed image.

Similarly to the case of the length of the boundary, the area of the damaged surface can be calculated by counting the number of “black” pixels, if one knows the scale at which the image was taken:

$$A = k^2 \cdot \sum_i^I \sum_j^J E(i, j) \quad \text{for } E(i, j) = 1 \quad (2)$$

where E is the value of the pixel (again only the pixels with value equal to unity $E(i,j) = 1$ (black pixels) are considered).

3.3. Characteristic pit/hole size

One of the goals of the study was to investigate whether the damage tends to cluster. To investigate whether new pits appear near the already present pits (what in time results in foil penetration and gradual formation of larger holes) or does the damage rather spread by forming new individual pits that weaken the structure and consequently form larger holes in just a few short steps. Additionally a question whether cavitation concentrates to the edge of a larger hole was posed. A parameter that can hold such information is the characteristic pit/hole size, defined as:

$$R = \frac{A}{L}, \quad (3)$$

where A is the damaged surface and L is the length of the boundary between the damaged and the undamaged surface.

The methods described above were employed for several series of images, each containing 200 images.

4. Results and discussion

It is well known that the intensity of cavitation erosion changes with distance from the piezo actuator [16]. We can expect that the most damage will occur in the vicinity of antinodes of the ultrasound standing wave [13].

To determine the best position of the aluminium foil, the relationship between the distance of the foil from the piezo actuator and the aggressiveness of erosion was studied. A rectangular strip of a foil was submerged into the vessel and exposed to ultrasound cavitation for 300 s. The damaged strip of foil was then examined (Fig. 5).

One can see that there is more than one region of increased erosion. The most damage occurs approximately at distances 0,

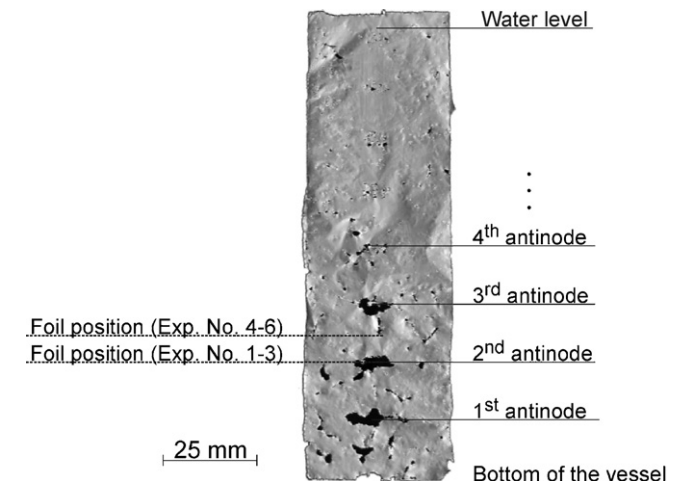


Fig. 5. Damaged strip of aluminium foil.

17, 32 and 48 mm from the bottom of the vessel, which approximately corresponds to the theoretical positions of antinodes (x_{an}) of ultrasound standing wave in water at 41.5 kHz [17]:

$$x_{an} = \lambda \cdot \frac{n}{2} = \frac{c}{f} \cdot \frac{n}{2}, \tag{4}$$

where λ is the wavelength, c is the sonic velocity in the fluid, f is the frequency and n is the antinode number ($n=0, 1, 2, \dots$). Eq. (4) gives values 0, 16.8, 33.7 and 50.6 mm for the antinode positions (0 mm corresponds to the bottom of the vessel).

We positioned the foil at two distances from the bottom of the vessel. The first position was near the antinode, at a distance of 32 mm, what resulted in the most aggressive cavitation. In the

other case was the foil positioned near the node at a distance of 40 mm from the bottom of the vessel, where the pressure oscillations are the smallest and the cavitation is not that aggressive. This way we obtained two different rates of damage:

- in the first case (near the antinode) a very short incubation period (short period when only pits are occurring) and extensive loss of material (large holes in the foil by the end of the experiment) was observed,
- in the second case (near the node) a very long incubation period (very long period when only pits are occurring) and limited loss of material (no or very small holes in the foil by the end of the experiment) was seen.

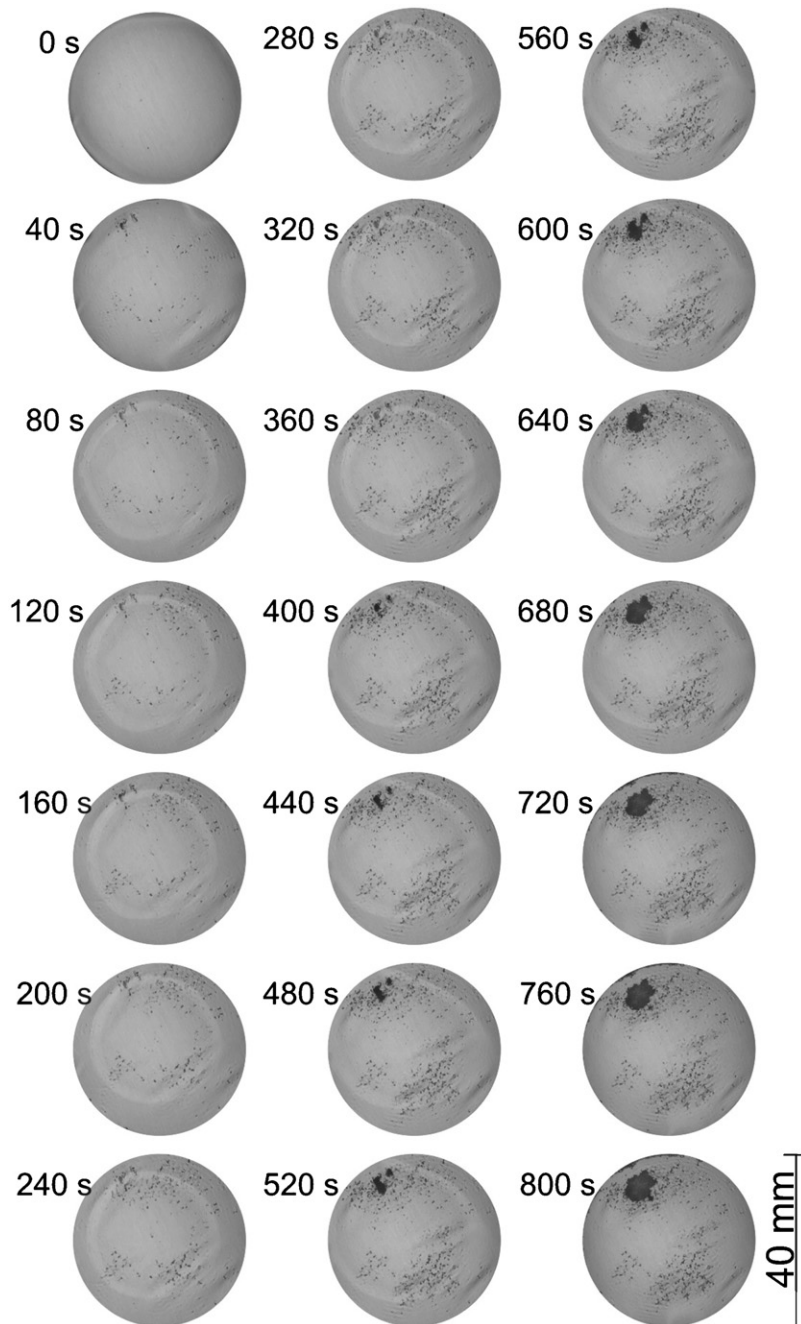


Fig. 6. Progression of damage on the foil for experiment No. 1.

For each of the two cases three 800 s long experiments were conducted (Nos. 1–3 at antinode and Nos. 4–6 at node).

4.1. Distance 32 mm from the bottom of the vessel

The foil was positioned near the antinode, hence the pressure oscillations were higher resulting in aggressive cavitation.

During experiments images of the foil were taken every 4 s for a period of 800 s. Fig. 6 shows a sequence of images taken during experiment No. 1 (only every 10th image is shown).

One can see that individual pits began to occur immediately after the exposure to the cavitation. Pits began to cluster in two regions at about the same distance from the centre of the foil (above and below). After about 200 s a hole appeared in the upper left side of the foil. After 400 s another hole on the right of the first one arose. Pitting became more intensive in the vicinity of both holes which resulted in their merging after 600 s of exposure to cavitation. Erosion progressed further until the experiment was stopped after 800 s. At the end, two damaged regions were present. The first one above the centre of the foil experienced erosion (appearance of holes in the foil), while only pits (plastic deformations that did not penetrate the foil) were present in the other one.

The reason for the difference in the aggressiveness of cavitation in these two regions is related to the following reasons:

- despite using a symmetrical vessel the ultrasonic field is probably not perfectly symmetrical,
- the surface of the foil could be damaged (small inaccuracies like scratches, dirt, pits, etc.) prior to the experiment,
- the upper region of damage lies a little bit closer to the edge of the foil, which could also act as a quasi-cavitation generator.

To quantify our visual observations, methods described in Section 3 were used. Length of the boundary between the damaged and the undamaged surface L (Eq. (1)), size of the damaged surface A (Eq. (2)) and characteristic pit/hole size R (Eq. (3)) were calculated for each image taken for the three experiments performed. Results are presented in diagrams in Fig. 7.

Each column presents results of measurements for one experiment. In the first row, results of edge length L are presented. Although the absolute values of the edge length differ between the experiments, an obvious common time evolution can be observed. The increase of edge length in time was low at the beginning and started to accelerate until it reached a point when it started to increase at a constant rate. The reason for this relationship is clear. Right at the beginning single pits in the foil were occurring and the edge length was increasing at a relatively low rate. After some time, the already present pits acted as cavitation generators that accelerated the damaging, but still only pits and no holes were appearing—the edge was growing at the fastest rate during that period. The period of accelerated damage boundary growth can be in fact related to the ending of the incubation period. Small pits clusters began to merge and the first holes appeared. Cavitation erosion then tended to concentrate to the edges of the holes, causing the decrease in the rate of the edge growth.

The second row represents the area of the damaged surface, again as a function of time. If one observes only the shape and not the absolute values, the diagrams are again very similar. The area of the damaged surface was increasing exponentially. As we already mentioned the first pits that occurred acted as cavitation generators that triggered appearance of more pits. As the incubation period passed, the rate of damage appearance increased further due to the separation of larger parts of the foil.

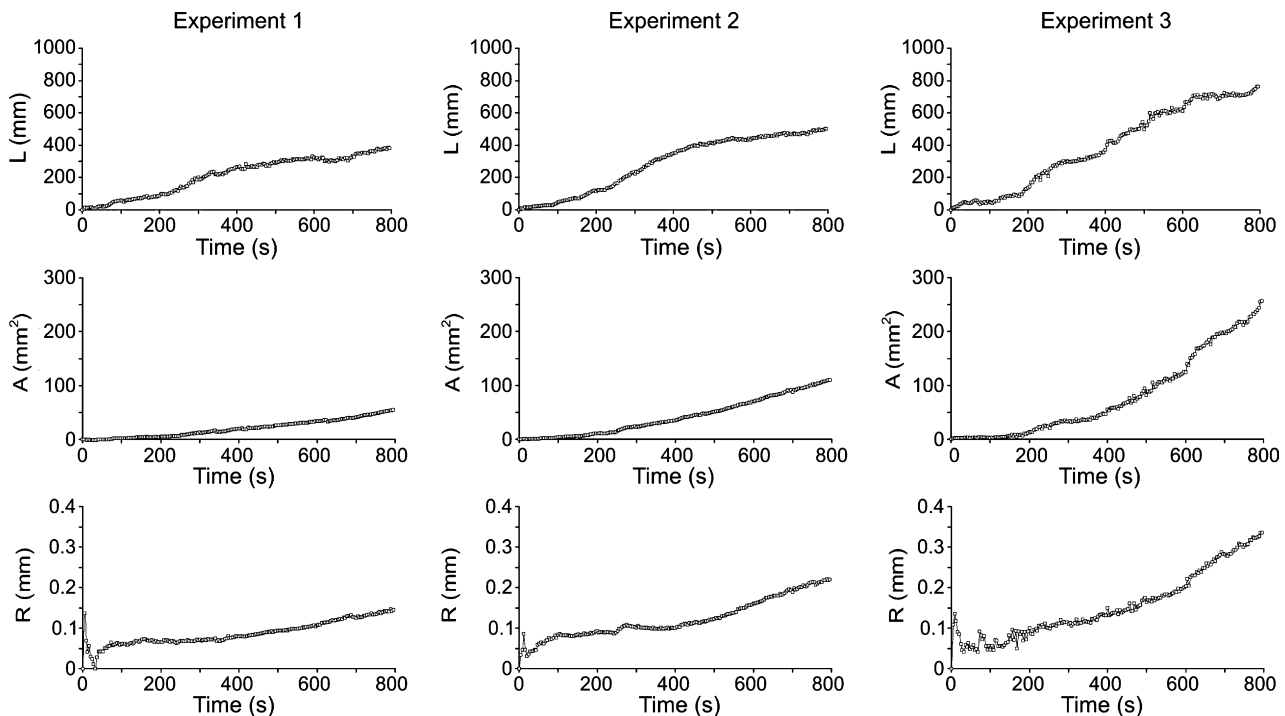


Fig. 7. Diagrams showing the time evolution of A , L and R for experiment Nos. 1–3.

The characteristic pit/hole size evolution is presented in the third row of Fig. 7. A value of $R=0$ was enforced when the boundary length L and damaged area A were 0 (this, of course, always occurred only in the first image in the series). It may not be as obvious as before but here also very similar trends can be seen. At first the characteristic size decreased exponentially, meaning that the edge of the pits/holes was growing faster than the area of the damaged surface. This was occurring prior to the appearance of the first holes in the foil and can therefore be characteristic for the incubation period. After that, a period of almost constant ratio between the damaged area and edge length could be observed—during this period pit clusters were appearing (this can be interpreted as the end of the incubation

period). Further on the characteristic pit/hole size began to grow exponentially—the area of the damaged surface grew faster than the edge length what can only be related to the appearance of larger holes in the foil and the fact that the erosion tends to concentrate to the edges of the holes.

4.2. Distance 40 mm from the bottom of the vessel

In this case the foil was positioned near the node. The pressure oscillations were lower, hence the cavitation was less aggressive. As in the case of aggressive cavitation (Section 4.1), three experiments were conducted at this distance of foil from the bottom of the vessel. Fig. 8 shows a reduced sequence of images from

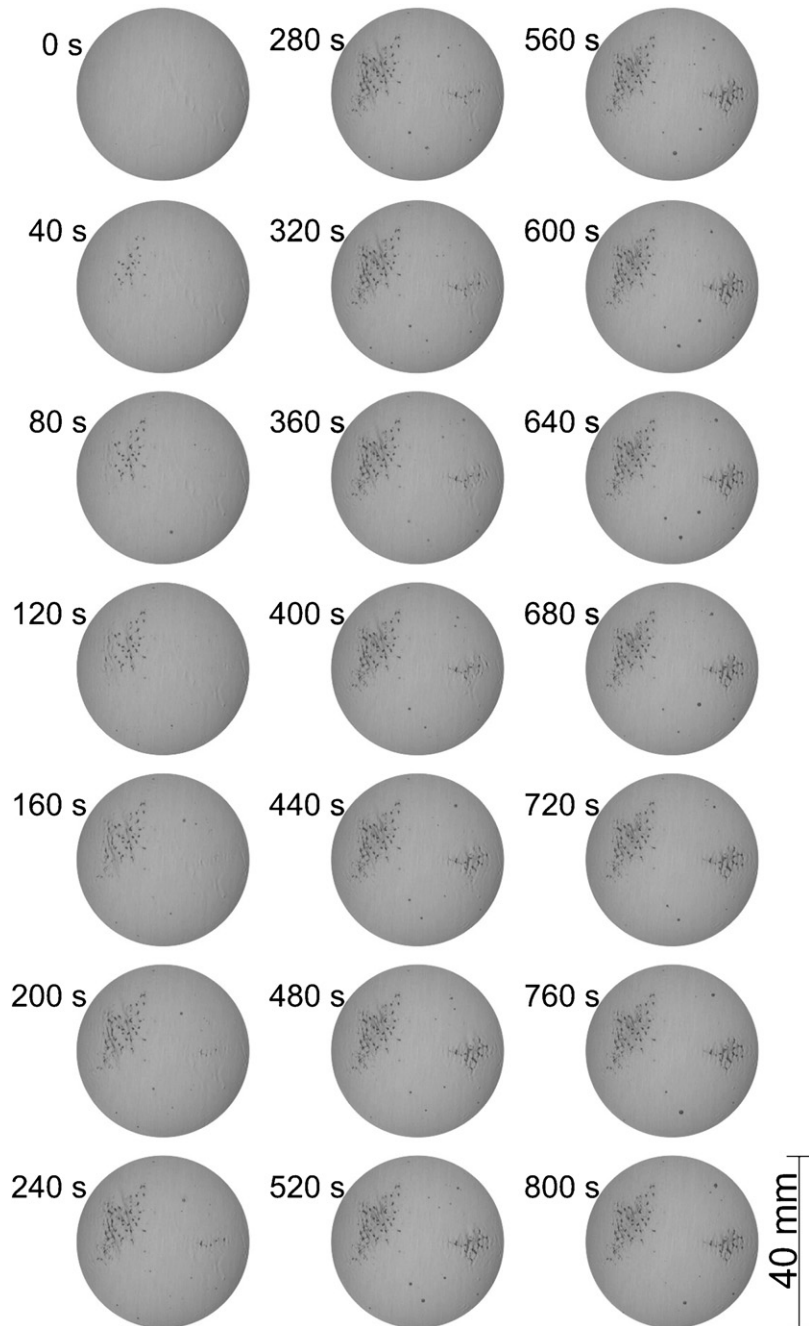


Fig. 8. Progression of damage on the foil for experiment No. 4.

the experiment No. 4 where only every 10th image in the series is shown.

Obvious, the cavitation during this experiment was less aggressive that during the experiment No. 1 (Section 4.1). This is because the foil was positioned closer to the node of the ultrasound standing wave. By assuring “gentler” cavitation conditions, the incubation period was prolonged to more than 800 s. This can be seen from Fig. 8 where no holes in the foil are present (only pits). The study of the incubation period of cavitation erosion is extremely important for further improvements of cavitation erosion models [18,19] and for better interpretation of short-term cavitation erosion measurements [9,20].

Again, two damaged regions can be seen. At the beginning pits occurred only in the upper right region, but after about 240 s pits began to cluster in the middle-right region as well what continued throughout the 800 s long experiment. If we were to extend the experiment further, we would very probably also experience cavitation erosion—formation of holes in the foil, but this has been already studied during experiments Nos. 1–3 (Section 4.1). The reasons behind the asymmetrical damage pattern are the same as for the previous set of experiments (Fig. 6): asymmetrical ultrasonic field, damaged surface of the foil and influence of inaccuracies of the aluminium foil mounting method.

Fig. 9 presents diagrams of the length of the boundary between the damaged and the undamaged surface L , size of the damaged surface A and the characteristic pit/hole size R for experiments Nos. 4–6.

The results in Fig. 9 are presented for the experiments Nos. 4–6, each presented by a column of diagrams. The differences in the shapes of the diagrams are more obvious in this set of experiments than in the previous one. If we first observe the length of the boundary between the damaged and the undamaged

surface L displayed in the first row, we see that in the case of experiment No. 4 the rate of increase of length decreased in time. Contrary to this, the rate remained approximately constant for the experiment No. 5 and increased for experiment No. 6. The reason is that the cavitation is less aggressive and even small differences in the position of the foil, evenness of the foil surface, dirt, etc., significantly influence the continuation of the experiment.

If the length of the boundary of the damaged surface from experiments Nos. 4 and 6 is examined, it can be seen that the trend of experiment No. 4 approximately (qualitatively) fits the first 350 s of the trend of the experiment No. 6, meaning that the damaging rate was somewhat higher in the last experiment (but the damage was still observed only in the incubation period).

Similarly, the damaged surfaces A (presented in the second row) display the same trend. For the experiment No. 4, the pitting stopped after about 300 s, for the experiment No. 5 the pitting continued at a constant rate and for the experiment No. 6 the pitting increased in time.

Nevertheless, when one observes the last row of diagrams where characteristic pit/hole size evolution is presented, very similar trends can be seen (as before the condition $R=0$ when $L=0$ and $A=0$ was enforced to avoid unphysical results). The ratio started from some point and exponentially decreased, meaning that the edges grew faster than the damaged area. As we learned before (Section 4.1), this type of trend can only be related to the incubation period of cavitation erosion. Moreover, if the diagrams of the characteristic pit/hole size R in Fig. 9 and the first period (about 50–100 s) of the diagrams of characteristic pit/hole size in Fig. 7 are compared, one sees that they qualitatively. For the cases of experiments Nos. 4–6 the values of R seem to converge to the same constant value—about $R=0.05$ mm. If we assume a circular shape of a pit, the final pit diameter can be

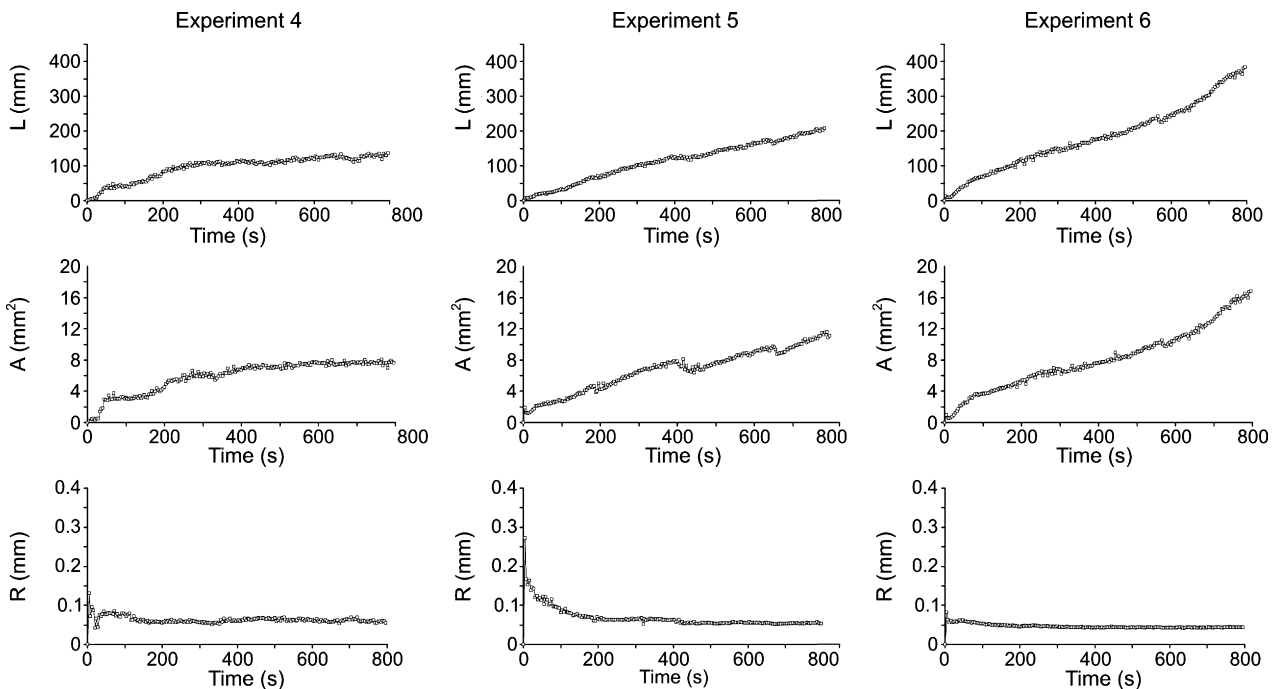


Fig. 9. Diagrams showing the time evolution of A , L and R for experiment Nos. 4–6.

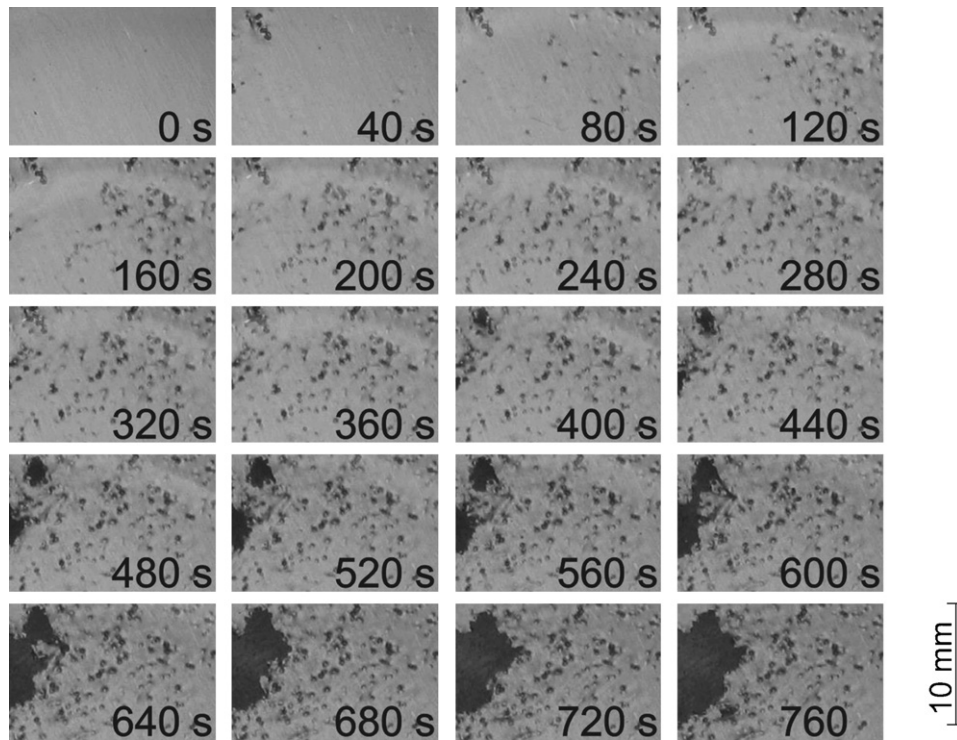


Fig. 10. Pit clustering in experiment No. 1.

calculated, resulting in 0.2 mm, what also agrees with the experiments performed by Dular et al. [9]. But we can claim (based on the results of experiments Nos. 1–3) that the erosion would not have stopped there and that the trend of the R would eventually start to grow if the tests had not been interrupted.

4.3. Pit clustering

We already mentioned that the pits tend to cluster and that the damage tends to progress the fastest in the region where a hole already exists (erosion of the edge of the hole). These two phenomena are once more presented in a sequence of magnified images from experiment No. 1 (Fig. 10). An image of the foil section taken every 40 s during the exposure to the cavitation is shown.

We can clearly see that individual pits started to damage the surface relatively evenly; hence we can conclude that the conditions for cavitation and damage appearance were favourable in the whole region of interest. After about 280 s, they began to concentrate in the upper left corner of the region, and eventually, after about 400 s, the first hole appeared. It is interesting that after that moment, individual pits appeared only in the closest vicinity of the growing hole—the most of erosion activity was concentrated to the edge of the hole. This observation again confirms that although the conditions were favourable in the whole region of interest, the new shape of the foil (with pits and holes) influenced the field—pits and especially holes locally acted as “cavitation generators” (it is known that the bubbles have a tendency to grow in small cracks—a phenomenon known as heterogeneous nucleation [2]) and triggered the formation of cavitation erosion clusters. Additional reason for the tendency

to first damage the edge of the holes is probably the decreased resistance of the material in that region.

5. Conclusions

The paper discussed phenomena that are considered obvious, but have in fact not been systematically studied yet. These are the tendency of cavitation damage to cluster, the tendency of cavitation to concentrate to the edges of the eroded holes and the self-amplification of the erosion rate.

By positioning the foil at various distances from the piezo actuator we were able to study two different cases of cavitation erosion. First we studied “real” erosion where holes in the foil appeared and the incubation period was relatively short. In the second set of experiments the incubation period was prolonged throughout the whole duration of the experiment to study pit clustering prior to the appearance of holes.

We found out that pits indeed tend to form clusters and that distinctive patterns of erosion progression exist. By measuring the damaged area and the length of the boundary between the damaged and the undamaged area the erosion mechanism (in terms of whether only individual pits or also erosion holes are appearing at a certain time) could be determined. A parameter of characteristic pit/hole size was introduced, what gave us an additional tool for the interpretation of the time evolution of the cavitation erosion.

Finally, clustering of pits was observed in a small region of interest. Pits were first appearing relatively evenly distributed over the whole region of interest. After the first holes appeared, the pits began to cluster in its immediate vicinity, although the flow conditions (pressure) for cavitation and consequently cav-

itation erosion were uniform prior to the appearance of pits and holes. It was concluded that the irregularities on the surface (for example, a hole) act as a promoter of cavitation, causing the bubbles to gather around them. It was also found that cavitation erosion tends to concentrate to the edges of the holes what can be explained by the fact that the material is weakened in that region.

The gained knowledge can be used for better prediction of cavitation erosion in experiments where the long-term erosion magnitude is approximated only on the base of observation within the incubation period [9]. The results can be also used for improvement of the present cavitation erosion models and consequently for more accurate CFD predictions of cavitation erosion [19,21].

The next step in the series of experiments that lead to a better understanding of cavitation erosion phenomenon is finding resemblance between the present results of ultrasound induced cavitation and the “real” hydrodynamic cavitation, therefore a series of long-term cavitation erosion tests in a hydraulic machine will be conducted.

References

- [1] B. Bachert, G. Ludwig, B. Stoffel, S. Baumgarten, Comparison of different methods for the evaluation of cavitation damaged surfaces, in: ASME Fluid Engineering Division Summer Meeting and Exhibition, Houston, 2005.
- [2] J.P. Franc, J.M. Michel, *Fundamentals of Cavitation*, Kluwer Academic Publishers, 2004.
- [3] B. Zeqiri, M. Hodnett, A.J. Carroll, Studies of a novel sensor for assessing the spatial distribution of cavitation activity within ultrasonic cleaning vessels, *Ultrasonics* 44 (2006) 73–82.
- [4] G.O.H. Whillock, B.F. Harvey, Ultrasonically enhanced corrosion of 304L stainless steel. II. The effect of frequency, acoustic power and horn to specimen distance, *Ultrason. Sonochem.* 4 (1997) 33–38.
- [5] T.B. Benjamin, A.T. Ellis, The collapse of cavitation bubbles and the pressures thereby produced against solid boundaries, *Philos. Trans. R. Soc. London* 260 (1966) 221–240.
- [6] M.S. Plesset, R.B. Chapman, Collapse of an initially spherical vapour cavity in the neighbourhood of a solid boundary, *J. Fluid Mech.* 47 (1971) 283–290.
- [7] J.L. Reboud, R. Fortes-Patella, A. Archer, Analysis of damaged surfaces. Part I. Cavitation mark measurements by 3D laser profilometry, in: 3rd ASME/JSME Joint Fluids Engineering Conference, San Francisco, 1999.
- [8] R.P. Tong, W.P. Schiffers, J.S. Shaw, J.R. Blake, D.C. Emmony, The role of splashing in the collapse of the laser-generated cavity near a rigid boundary, *J. Fluid Mech.* 380 (1999) 339–361.
- [9] M. Dular, B. Bachert, B. Stoffel, B. Širok, Relationship between cavitation structures and cavitation damage, *Wear* 257 (2004) 1176–1184.
- [10] Y. Ito, R. Oba, Comparison between four practical methods to detect the erosive area in cavitating flows, in: Proceedings of the XVII IAHR Symposium, Beijing, 1994.
- [11] R. Simoneau, Cavitation pit counting and steady state erosion rate, in: International Symposium on Cavitation, Deauville, 1995.
- [12] J.-L. Laborde, C. Bouyer, J.-P. Caltagirone, A. Gérard, Acoustic cavitation field prediction at low and high frequency ultrasounds, *Ultrasonics* 36 (1998) 581–587.
- [13] D. Krefting, R. Mettin, W. Lauterborn, High-speed observation of acoustic cavitation erosion in multibubble systems, *Ultrason. Sonochem.* 11 (2004) 119–123.
- [14] F. Brand, Ein physikalisches Verfahren zur Bestimmung von gelösten und ungelösten Gasen in Wasser, *Voith Forschung und Konstruktion* 27 (1981).
- [15] I. Sobel, Neighborhood coding of binary images for fast contour following and general array binary processing, *Comput. Graph. Image Process* 8 (1978) 127–135.
- [16] V. Sáez, A. Frías-Ferrer, J. Iniesta, J. González-García, A. Aldaz, E. Riera, Characterization of a 20 kHz sonoreactor. Part I. Analysis of mechanical effects by classical and numerical methods, *Ultrason. Sonochem.* 12 (2005) 59–65.
- [17] J. Billingham, A.C. King, *Wave Motion*, Cambridge University Press, 2000.
- [18] R. Fortes-Patella, J.L. Reboud, L. Briançon-Marjolle, A phenomenological and numerical model for scaling the flow aggressiveness in cavitation erosion, Workshop on Cavitation Erosion, Bassin d’essais des carenes, Val de Reuil, 2004.
- [19] M. Dular, B. Stoffel, B. Širok, Development of a cavitation erosion model, *Wear* 261 (2006) 642–655.
- [20] B. Bachert, G. Ludwig, B. Stoffel, B. Širok, M. Novak, Experimental investigations concerning erosive aggressiveness of cavitation in a radial test pump with the aid of adhesive copper films, in: 5th International Symposium on Cavitation, Osaka, 2003.
- [21] M. Dular, B. Širok, B. Stoffel, Experimental and numerical modeling of cavitation erosion, in: 6th International Symposium on Cavitation, Wegeningen, 2006.